

# Nanoscale

Accepted Manuscript



This is an *Accepted Manuscript*, which has been through the Royal Society of Chemistry peer review process and has been accepted for publication.

*Accepted Manuscripts* are published online shortly after acceptance, before technical editing, formatting and proof reading. Using this free service, authors can make their results available to the community, in citable form, before we publish the edited article. We will replace this *Accepted Manuscript* with the edited and formatted *Advance Article* as soon as it is available.

You can find more information about *Accepted Manuscripts* in the [Information for Authors](#).

Please note that technical editing may introduce minor changes to the text and/or graphics, which may alter content. The journal's standard [Terms & Conditions](#) and the [Ethical guidelines](#) still apply. In no event shall the Royal Society of Chemistry be held responsible for any errors or omissions in this *Accepted Manuscript* or any consequences arising from the use of any information it contains.

## COMMUNICATION

# Hydrogen-Induced Structural Transformation of AuCu Nanoalloys Probed by Synchrotron X-ray Diffraction Techniques

Cite this: DOI: 10.1039/x0xx00000x

M. Yamauchi,<sup>\*,a,b</sup> K. Okubo,<sup>a,b</sup> T. Tsukuda,<sup>c,d</sup> K. Kato,<sup>\*,b,e</sup> M. Takata,<sup>e</sup> and S. Takeda<sup>f</sup>Received 00th January 2012,  
Accepted 00th January 2012

DOI: 10.1039/x0xx00000x

www.rsc.org/

**In situ X-ray diffraction measurements reveal that the transformation of a AuCu nanoalloy from a face-centered-cubic to an L1<sub>0</sub> structure is accelerated under hydrogen atmosphere. The structural transformation rate for the AuCu nanoalloy under hydrogen above 433 K was found to be 100 times faster than that in vacuum, which is the first quantitative observation of hydrogen-induced ordering of nanoalloys.**

The ordering of constituent elements in a lattice exerts an enormous influence on the physical and chemical properties of alloys. The L1<sub>0</sub>-type structure is a typical example in which layers of constituent elements are alternately stacked as exemplified in Figure 1 for a Au-Cu nanoalloy (NA). Previous studies have shown that regulation of the elemental arrangement is a primary factor in the functionalization of NA materials; Fe-Pt,<sup>1</sup> Fe-Pd,<sup>2</sup> and Fe-Ni NAs,<sup>3</sup> with a tetragonal L1<sub>0</sub> structure show ferromagnetism, and ordered NAs exhibit excellent catalytic properties.<sup>4,5</sup>

In general, ordered alloy phases emerge during high-temperature treatments of the corresponding disordered alloy.<sup>1</sup> However, high-temperature treatments applied to nanometer-sized materials often diminish their potential capabilities because sintering occurs. To overcome this problem, Schaak and coworkers<sup>6</sup> synthesized ordered Au-Cu NAs in solution at temperatures lower than those used for preparation in metallurgical techniques. As an alternative approach, a method of annealing NAs under hydrogen has been developed. Using this method, the temperature required for a structural transformation of the disordered to ordered phase in an Fe-Pt NA, for example, could be reduced from 823 to 553 K under hydrogen atmosphere.<sup>7</sup> B2-type Cu-Pd NAs were obtained at 373–423 K.<sup>8</sup> Recently, Bloch et al.<sup>9</sup> reported an acceleration in the ordering of Fe-V alloys. These hydrogen-induced structural

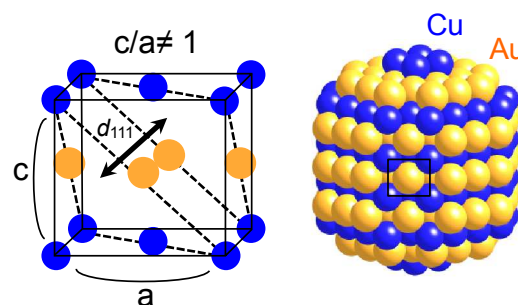


Figure 1. Elemental arrangements in the ordered L1<sub>0</sub> lattice of a Au-Cu nanoalloy: the {111} planes are shown by the dotted lines. The yellow and blue spheres represent Au and Cu atoms, respectively.

transformations are based on the strong affinities of Pt, Pd, and V with hydrogen.

The question that then arises is, can we apply the hydrogen treatment method to other alloys composed of metals that interact weakly with hydrogen? Interestingly, it has been demonstrated that some nanometer-sized metals and alloys can store hydrogen, whereas this is not possible in the bulk state.<sup>10</sup> These observations hint at the possibility that this hydrogen exposure treatment can be applied to control the atomic-level structure of a wide variety of NAs. We report herein the successful production of a AuCu (1:1) NA with an L1<sub>0</sub> structure by hydrogen exposure treatment; both Au and Cu interact only weakly with hydrogen under ambient conditions. We also studied the kinetics of the AuCu-NA structural transformation using a synchrotron-based in-situ X-ray diffraction (XRD) technique to obtain an insight into the mechanism.

As reported previously,<sup>8</sup> the key to producing ordered NAs is the preparation of atomically-well-mixed alloys as precursors. To this end, we prepared AuCu NAs by the rapid and simultaneous reduction of Au and Cu ions (1:1) using a strong reducing agent NaBH<sub>4</sub>. Poly[vinyl-2-pyrrolidone] was used as a stabilizer against sintering. Transmission electron microscope (TEM) images (Figure S1(a)) of the NA specimens revealed the formation of nanoparticles with an average diameter of 3.4 ± 0.8 nm. The actual alloy composition was found to be Au:Cu = 55.0:45.0 by

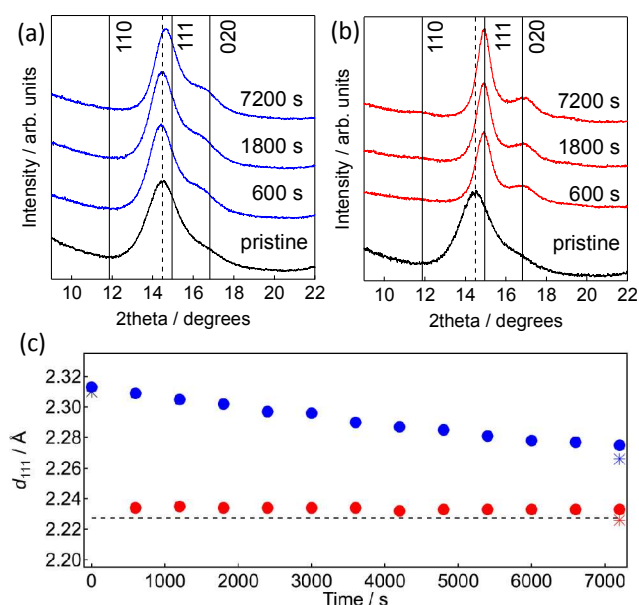


Figure 2. XRD patterns of the AuCu NAs under (a) vacuum and (b) 100 kPa of  $H_2$  at 453 K using an imaging plate. The dotted lines indicate the 111 diffraction peak position in the XRD pattern of the pristine NA evacuated at 300 K. Each solid line is located at the 110, 111, or 020 diffraction positions for the bulk  $L_{10}$  AuCu. (c) Time dependence of the (111) interplanar spacing ( $d_{111}$ ) of the AuCu NA under vacuum (●) and hydrogen (●) at 453 K estimated from the 111 diffraction position in the XRD pattern. The  $d_{111}$  of the pristine AuCu NA (\*), AuCu NAs after heated to 453 K for 7200 s under vacuum (\*) and hydrogen (\*), which were calculated from the 111 diffraction positions in XRD patterns measured at 300 K.

inductively coupled plasma atomic emission spectroscopy (ICP-AES) analysis. The XRD pattern of the AuCu NAs measured on a lab-based XRD diffractometer with Cu K $\alpha$  radiation indicated a single face-centered-cubic (fcc) phase, suggesting that the prepared NA is a solid-solution-type alloy. The lattice constant was determined to be 4.017(1) Å by Rietveld analysis, which is larger than the average of the individual lattice constants of Au and Cu (3.85 Å). The oxidation state of the AuCu NA was examined by X-ray photoelectron spectroscopy. Binding energy peaks of Au 4f<sub>5/2, 7/2</sub> for the AuCu NA were located at almost the same binding energies as those for the Au nanoparticle (Figure S2(a)). Furthermore, the Cu 2p<sub>3/2</sub> peak for the AuCu NA was observed at the same energy as that for bulk Cu (Figure S2(b)). These results suggest that the AuCu NA is in a metallic state and the relatively large lattice constant of the pristine NA cannot be attributed to presence of oxide species in the NA. Lattice expansion has been predominantly observed in solid processed by severe plastic deformation processing.<sup>11</sup> We think, therefore, that the NAs prepared at low temperatures are in a non-equilibrium state, which contains internal defects, such as point defects, atomic displacement, lattice distortion and so on.<sup>12</sup>

Time courses of the XRD patterns of the AuCu NA heated under vacuum and hydrogen atmosphere were obtained in situ using the Debye-Scherrer camera installed on the BL44B2 beamline<sup>13</sup> at SPring-8, Japan. The XRD pattern was measured every 10 min (600 s) after the X-ray shutter has opened. Figures 2(a) and (b) show typical XRD patterns recorded at 453 K under vacuum and 100 kPa of hydrogen, respectively. The positions of the 111

peak in the patterns measured under vacuum did not change considerably from that observed for the pristine NA. In sharp contrast, the 111 peak position under 100 kPa of hydrogen was shifted to higher angles compared to those under vacuum. In addition to 111 and 020 peaks, we were able to identify a new diffraction peak for the hydrogen-treated sample at an angle where 110 diffraction from the  $L_{10}$  phase is observable although the diffraction peak was broadened resulting from small crystal sizes.<sup>14</sup> In order to compare more quantitatively the structural change behavior, the (111) interplanar spacing ( $d_{111}$ ), illustrated in Figure 1, was calculated from the 111 diffraction position and is plotted as a function of time in Figure 2(c). Because both fcc and  $L_{10}$  structures have {111} planes in their unit cells, we think that  $d_{111}$  values can be a suitable indicator to show successive transformation from fcc to  $L_{10}$  phase. It is notable that the  $d_{111}$  of the AuCu NAs after exposure to hydrogen approached the value of bulk  $L_{10}$ -type AuCu even at the first measurement point, i.e., 600 s and became almost constant after that. The  $d_{111}$  of the hydrogen-treated AuCu NA determined at 300 K was almost the same as that of bulk  $L_{10}$  AuCu. This result strongly suggests that both structural transformation and ordering of AuCu NAs are accelerated by the hydrogen treatment. Further, we conducted Rietveld profile analyses of the XRD patterns measured under hydrogen as shown in Figure S3 and determined structural parameters of the  $L_{10}$  phase, such as, lattice constants, the site occupancy by an element and the mass ratio of the  $L_{10}$  phase in the NA. These structural parameters are plotted against time in

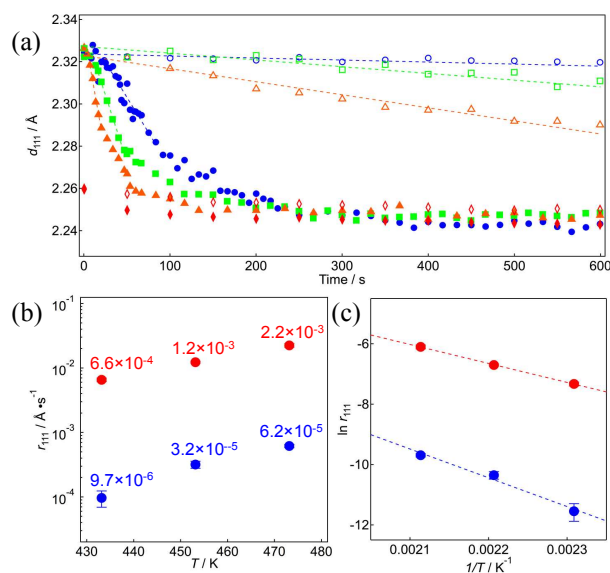


Figure 3. (a) Time dependence of the (111) interplanar spacing ( $d_{111}$ ) for samples heated at 433 (blue circles), 453 (green squares), 473 (orange triangles) and 573 K (red diamonds) under vacuum (open symbols) and 100 kPa of  $H_2$  (filled symbols). The fit of the initial linear part, shown as dotted lines, was used to determine the initial structural transformation rate ( $r_{111}$ ). (b) Temperature dependence and (c) Arrhenius plot of the  $r_{111}$  values under vacuum (blue) and 100 kPa of  $H_2$  (red). Activation energies for the structural transformation are estimated by a least mean square fit, as shown by the dashed lines.

inset of Figure S3. It is notable that the  $L_{10}$  phase having lattice constants similar to those of the bulk counterpart is formed at the first measurement point, i.e., 600 s. The mass ratio of the  $L_{10}$  phase and the site occupancy attained 55 and 86 %, respectively, at 1200 s, and became almost constant after that. This result would indicate that ordering in the AuCu NA starts with short-range atomic rearrangement, which maybe completed in a relatively short time. Considering a large volume percentage of surface portions existing in particles of diameters less than 2-3 nm, such as edges and corners, it is probable that the complete transformation to the ordered phase hardly occurs without greater structural transformation accompanied by particle growth.<sup>15</sup> Additionally, we confirmed that the 2 h hydrogen treatment at 453 K did not cause heavy aggregation of the AuCu NAs (Figure S1(b)), which is an advantage of this low-temperature method.

The XRD measurement employing an imaging plate proved formation of  $L_{10}$  phase in NAs. Kinetic information, however, was hardly given by this method. Then, we applied a flat-panel sensor as a detector for a very short-period measurement. The system layout is given in Figure S4. The XRD patterns were collected with a time resolution of 0.333 sec by using a flat panel sensor. Several XRD patterns measured at 433, 453, 473 and 573 K are shown in Figure S5. At 433 K, we note that the 111 peak under hydrogen has been shifted to a higher angle even at 66.6 s, and this displacement increased over time (Figure S5(a)). Similar behavior was observed in the patterns of the AuCu NAs treated at 453 and 473 K (Figure S5(b) and (c)). In contrast, the difference in the 111 peak positions between the two conditions at 573 K was relatively small over the experimental time (Figure S5(d)). The  $d_{111}$  values of the samples heated to 433, 453, and 473 K under vacuum decreased linearly and the rate of decrease was larger for higher temperatures. The  $d_{111}$  value for the sample heated under hydrogen decreased much faster than that heated under vacuum, and reached a plateau. The reduction rate ( $r_{111}$ ) was obtained by fitting the data at the initial stage of the heating with a linear function and is plotted in Figure 3(b). Notably, the  $r_{111}$  values under hydrogen atmosphere are two orders of magnitude larger than those under vacuum regardless of the temperatures. Another feature is that the  $r_{111}$  values increase with

the temperature. We estimated the activation energy of the structural transformation ( $E_a$ ) from a least mean square analysis of the Arrhenius plot of the  $r_{111}$  value (Figure 3(c)). The  $E_a$  values under vacuum and hydrogen were found to be  $0.82 \pm 0.11$  and  $0.54 \pm 0.06$  eV, respectively, which demonstrates that hydrogen exposure treatment reduces the activation barrier for the structural transformation of NAs. This is the first quantitative observation of acceleration of atomic rearrangement of NAs under hydrogen atmosphere.

At this stage, there are still questions about how hydrogen induces the structural transformation in AuCu NAs. For example, does the AuCu NA absorb hydrogen?, and if so, how large amount of hydrogen is absorbed? The H concentration in the AuCu NA heated at 453 K was investigated by measuring hydrogen pressure-composition (PC) isotherms. The PC isotherms were measured three times successively and are indicated in Figure 4. In the first absorption measurement, the H concentration increased in a pressure region of 1 to 5 kPa and, at 100 kPa, reached 0.027 H per hypothetical AuCu atom with an average atomic weight between that of Au and Cu. This H concentration is much smaller than those in hydrides of nanoparticles, e.g., 0.22, 0.23, and 0.29 H per Pd, Rh and PdRh atom, respectively.<sup>16</sup> In the desorption process, the H concentration did not decrease considerably, and  $\sim 0.01$  H per metal atom remained inside the sample. There was little increase in the H concentration during the second and third runs,<sup>17</sup> implying that the AuCu NA absorb only a very small amount of H at 453 K but does not release it completely.

To clarify the H absorption site, we conducted  $^2\text{H}$  wide-line and  $^2\text{H}$  magic-angle-spinning (MAS) NMR measurements of the AuCu NA exposed to deuterium gas at 453 K for 2 h. Noticeable signals, however, were not observed in either measurements (Figure S6). The maximum H concentration in the AuCu NA, i.e., 0.027 H per metal atom corresponds to 0.02 wt.% of the sample, which is close to the  $^2\text{H}$  NMR detection limit for broad deuterium signals.<sup>18</sup> These results suggest an infinitesimal quantity of hydrogen induces the structural transformation in AuCu NAs. In addition, no sharp NMR signals were observed for the AuCu NA evacuated after deuterium exposure treatment, indicating that there is no molecular hydrogen adsorbed via physical interaction in the samples.

On the basis of the data obtained, we also considered the structural transformation mechanism in the presence of hydrogen. To achieve ordering in NAs, randomly arranged metal atoms should be moved to specific lattice points. The formation energy of  $L_{10}$ -type AuCu can be divided into two parts, i.e., elastic and chemical parts. Ordering in the AuCu alloys is prompted when elastic formation energy (loss) for structural transformation is compensated by energetic gain brought by thermal energy and chemical formation energy among unlike metals via charge transfer.<sup>19, 20</sup> As shown in Figure 3 (a), the  $d_{111}$  of the AuCu NAs heated to 573 K under vacuum was significantly small compared to that of the pristine NA even at the first measurement point, which indicates that thermal energy is sufficiently supplied to the NAs for the structural transformation at 573 K. It is notable that the reduction of the  $d_{111}$  of the AuCu

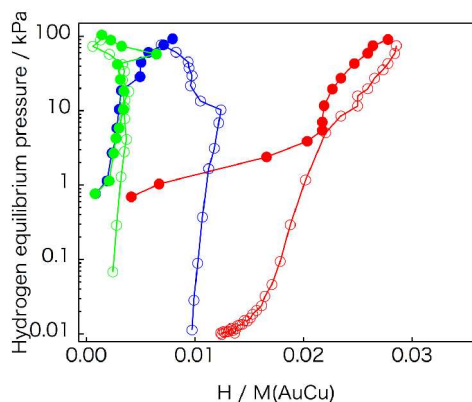


Figure 4. Hydrogen pressure-composition isotherms of the AuCu NA measured at 453 K. Red, blue and green curves correspond to isotherms obtained in the first, second, and third measurements, respectively. Data obtained in the absorption and desorption process are denoted by filled and open circles, respectively.

NA exposed to hydrogen occurred faster than that under vacuum at this temperature. Therefore, we think that a role of hydrogen is not only generation of lattice strain but also promotion of structural transformation through certain chemical interaction, e.g., a mediation of charge transfer between Au and Cu. Further investigation for the mechanistic understanding of the hydrogen-induced structural transformation of NAs is underway.

## Conclusions

In situ X-ray diffraction measurements clarified that the structural transformation rate under hydrogen above 433 K is 100 times faster than that in vacuum, which represents the first quantitative observation of the efficiency of hydrogen exposure treatment for the structural transformation and ordering of NAs. Hydrogen pressure-composition isotherms proved that hydrogen concentration in the AuCu NA was 0.027 H per metal atom. These results indicate that a very small amount of hydrogen can promote atomic rearrangement even in hydrogen-inactive AuCu NAs. Therefore, hydrogen exposure treatment can be applied to a variety of alloys including non-hydrogen storage alloys, which will contribute to further functionalization of nanoscale materials.

## Acknowledgement

This work was partly supported by JST-CREST and JSPS KAKENHI Grant Number 24655040 and 25288030. The synchrotron radiation experiments were performed on the BL44B2 beamline at the SPring-8 with the approval of RIKEN (Proposal No. 20100075). The in-situ experiments using the flat panel sensor were supported by Mr. Michitaka Takemoto (Japan Synchrotron Radiation Research Institute).

<sup>a</sup> WPI-I2CNER, Kyushu University, Motooka 744, Nishi-ku, Fukuoka 819-0395, Japan

<sup>b</sup> CREST, JST, 4-1-8 Honcho, Kawaguchi, Saitama 332-0012, Japan

<sup>c</sup> Department of Chemistry, School of Science, The University of Tokyo, Hongo 7-3-1, Bunkyo-ku, Tokyo 113-0033, Japan

<sup>d</sup> Elements Strategy Initiative for Catalysts and Batteries (ESICB), Kyoto University, Katsura, Kyoto 615-8520, Japan

<sup>e</sup> RIKEN SPring-8 Center, 1-1-1 Kouto, Sayo-cho, Sayo-gun, Hyogo 679-5148, Japan

<sup>f</sup> Department of Chemistry, Faculty of Science, Hokkaido University, Nishi 8, Kita 10, Kita-ku, Sapporo 060-0810, Japan

†Electronic Supplementary Information (ESI) available: [Detailed methods and results including the synthetic method, TEM images, XRD patterns, and <sup>2</sup>H NMR spectra.]. See DOI: 10.1039/c000000x/

## References

- S. Sun, C. B. Murray, D. Weller, L. Folks, A. Moser, *Science* 2000, **287**, 1989; Z. R. Dai, S. Sun, Z. L. Wang, *Nano Lett.*, 2001, **1**, 443-447; D. Weller, A. Moser, L. Folks, M. E. Best, W. Lee, M. F. Toney, M. Schwickert, J-U. Thiele, M. F. Doerner, *IEEE Trans. Magn.*, 2000, **36**, 10-15; Delalande, M. J. -F. Guinel, L. F. Allard, A. Delattre, R. L. Bris, Y. Samson, P. Bayle-Guillemaud, P. Reiss, *J. Phys. Chem. C*, 2012, **116**, 6866.
- C. Issro, M. Abes, W. Püschl, B. Sepiol, W. Pfeiler, P. F. Rogl, G. Schmerber, W. A. Soffa, R. Kozubski, V. Pirron-Bohnes, *Mater. Trans. A*, 2006, **37A**, 3415; N. Sakuma, T. Ohshima, T. Shoji, Y. Suzuki, R. Sato, A. Wachi, A. Kato, Y. Kawai, A. Manabe, T. Teranishi, *ACS Nano*, 2011, **5**, 2806; Y. Yu, K. Sun, Y. Tian, X. -Z. Li, M. J. Kramer, D. J. Sellmyer, J. E. Shield, S. Sun, *Nano Lett.*, 2013, **13**, 4975-4979.
- L. Néel, J. Pauleve, R. Pauthenet, J. Laugier, D. Dautreppe, *J. Appl. Phys.*, 1964, **35**, 873; M. Kotsugi, C. Mitsumata, H. Maruyama, T. Wakita, T. Taniuchi, K. Ono, M. Suzuki, N. Kawamura, N. Ishimaru, M. Oshima, Y. Watanabe, M. Taniguchi, *Appl. Phys. Exp.*, 2010, **3**, 013001.
- D. Wang, H. L. Xin, R. Hovden, H. Wang, Y. Yu, D. A. Muller, F. J. DiSalvo, H. D. Abruna, *Nat. Mater.*, 2013, **12**, 81; E. Casado-Rivera, D. J. Volpe, L. Alden, C. Lind, C. Dowine, T. Vazquez-Alvarez, A. C. D. Angelo, F. J. DiSalvo, H. D. Abruna, *J. Am. Chem. Soc.*, 2004, **126**, 4043.
- J. Yang, X. Chen, X. Yang, J. Y. Ying, *Energy Environ. Sci. Technol.*, 2012, **5**, 8976.
- R. E. Schaak, A. K. Sra, B. M. Leonard, R. E. Cable, J. C. Bauer, Y. -F. Han, J. Means, W. Teizer, Y. Vasquez, E. S. Funk, *J. Am. Chem. Soc.*, 2005, **127**, 3506; A. K. Sra, R. E. Schaak, *J. Am. Chem. Soc.*, 2004, **126**, 6667. S. Sra, K. Amadeep, T. D. Ewers, R. E. Schaak, *Chem. Mater.*, 2005, **17**, 758.
- M. Nakaya, M. Kanehara, M. Yamauchi, H. Kitagawa, T. Teranishi, *J. Phys. Chem. C*, 2007, **111**, 7231.
- M. Yamauchi, T. Tsukuda, *Dalton Trans.*, 2011, **40**, 4842; M. Okada, A. Kamegawa, J. Nakahigashi, A. Yamaguchi, A. Fujita, M. Yamauchi, *Mater. Sci. Eng. B*, 2010, **173**, 253-259.
- J. Bloch, O. Levy, B. Pejova, J. Jacob, S. Curtarolo, B. Hjörvarsson, *Phys. Rev. Lett.*, 2012, **108**, 215503.
- H. Kobayashi, H. Morita, M. Yamauchi, R. Ikeda, H. Kitagawa, Y. Kubota, K. Kato, M. Takata, *J. Am. Chem. Soc.*, 2011, **133**, 11034; H. Kobayashi, M. Yamauchi, H. Kitagawa, *J. Am. Chem. Soc.*, 2012, **134**, 6893-6895.
- G. K. Rane, U. Welzel, S. R. Meka, E. J. Mittemeijer, *Acta Mater.* 2013, **61**, 4524-4533; P. Sharma, K. Biswas, A. K. Mondal, K. Chattopadhyay, *Scr. Mater.*, 2009, **61**, 600-603.
- M. Yamauchi, H. Kobayashi, H. Kitagawa, *ChemPhysChem*, 2009, **10**, 2566; M. Yamauchi, R. Ikeda, H. Kitagawa, M. Takata, *J. Phys. Chem. C* 2008, **112**, 3294; T. Kandemir, F. Girgsdies, T. C. Hansen, K. -D. Liss, I. Kasatkin, E. L. Kunkes, G. Wowsnick, N. Jacobsen, R. Schlögl, M. Behrens, *Angew. Chem. Int. Ed.*, 2013, **52**, 5266-5170; E. Wetterskog, C. -W. Tai, J. Grins, L. Bergström, G. Salazar-Alvarez, *ACS Nano*, 2013, **7**, 7132-7144.
- K. Kato, R. Hirose, M. Takemoto, S. Ha, J. Kim, M. Higuchi, R. Matsuda, S. Kitagawa, M. Takata, *AIP Conf. Proc.*, 2010, **1234**, 875.
- B. E. Warren, *Prog. Met. Phys.*, 1959, **8**, 147-202.
- C. Rong, D. Li, V. Nandwana, N. Poudyal, Y. Ding, Z. L. Wang, H. Zeng, J. P. Liu, *Adv. Mater.*, 2006, **18**, 2984-2988; V. Shah, L. Yang, *Philos. Mag. A.*, 1999, **79**, 2025.

Journal Name

- 16 H. Kobayashi, H. Morita, M. Yamauchi, R. Ikeda, H. Kitagawa, Y. Kubota, K. Kato, M. Takata, S. Toh, S. Matsumura, *J. Am. Chem. Soc.*, 2012, **134**, 12390.
- 17 A slight deviation of the measurement conditions could influence the result considerable. In this measurement setting, 0.01 H per metal atom is probably the detection limit.
- 18 L. J. Mathias, R. D. Davis, S. J. Steadman, W. L. Jarrett, *Macromolecules*, 2004, **37**, 3699.
- 19 M. Kuhn, T. K. Sham, *Phys. Rev. B*, 1994, **49**, 1647.
- 20 D. Paudyal, A. Mookerjee, *Physica B*, 2005, **366**, 55-61.